International Journal of Heat and Mass Transfer 52 (2009) 4008–4020

Contents lists available at ScienceDirect

International Journal of Heat and Mass Transfer

journal homepage: www.elsevier.com/locate/ijhmt

Vector lines and potentials for computational heat transfer visualisation

G.D. Mallinson *

Department of Mechanical Engineering, The University of Auckland, Auckland, New Zealand

ARTICLE INFO

Article history:
Received 6 January 2009
Accepted 23 March 2009
Available online 4 May 2009

Keywords:
Streamlines
Heat lines
Computational heat transfer visualisation
Vector potentials
Scalar stream functions
Transport vector

ABSTRACT

Since the development of 3D computational heat transfer in the early 1970s, construction of the lines of vector fields has been a fundamental visualisation technique. In addition to the usual velocity lines, the lines of transport vectors for mass, energy and entropy can be especially relevant to heat and mass transfer. The use of scalar stream functions and vector potentials to ensure that these lines satisfy flux conservation is discussed in this paper by tracing the history of their use for streamline construction. A flux conservative method that uses an energy vector potential for constructing energy transport lines is described and its use for constructing 3D heat lines is demonstrated for natural convection in a cavity.

1. Introduction

1.1. History

From the early beginnings of computational fluid dynamics and heat transfer (CFD/CHT), visualisation of the numerical solution fields has been almost as important as the solution processes themselves. The crux of the matter is that for 3D flows there is no suitable "whole field" method of flow visualisation as there is for 2D flow. Moreover, the most obvious method, that of constructing vector lines, is susceptible to errors arising from the forward stepping nature of the integration procedure and inaccurate interpolation of the numerical vector fields.

Prior to the development of 3D computational heat transfer, the stream function – vorticity method was very popular and the stream function trivially provided a whole field method of flow visualisation. Stream function contour lines are the lines the velocity or mass flux vector field and the difference between the stream function values of two lines is equal to the volume or mass flow between them.

Vector potentials or dual scalar stream functions can be used to represent 3D vector fields and early CHT solutions (Holst and Aziz [1], Mallinson and de Vahl Davis [2]) of 3D natural convection cavity flows used vector potential – vorticity methods. However there is no direct relationship between the vector potential and the lines of the velocity field that it represents. Visualisations of these solutions used planar maps and lines of the velocity vector fields. In practice issues associated with the prescription of boundary conditions for the vector potential and its lack of utility for visualisation meant that the vector potential – vorticity method has been almost completely bypassed in favour of primitive variable CHT methods.

Unlike the vector potential, dual stream functions do have a direct relationship with the lines of the vector field they represent. The directions of their gradients are normal to these lines and, in a manner similar to the 2D stream function, areas in stream function coordinates are proportional to the vector flow rates. Tantalising as this relationship might seem, the mathematical complexity of this relationship has precluded the development of a workable whole field visualisation strategy. Nevertheless, the search for an appropriate methodology has continued since the early 1970s when the challenges of 3D visualisation became apparent.

From the author's perspective, this search started with the realisation that potentials of some kind were necessary to ensure that interpolations of a discrete velocity field were mass conservative. As will be described in this paper a vector potential, trivially available as part of a vector potential – vorticity solution, can be used to provide mass conservative interpolations of a velocity or mass flux field. The desire to provide mass conservative interpolations from face centred staggered velocity fields used by PHOENICS (Spalding [3]) and its precursors led to the development of an algorithm, represented later in this paper, that used these data to integrate path lines analytically across each computational cell. This algorithm was embedded in GRAFFIC, (Mallinson [4]) which was first applied by Pollard and Spalding [5] to visualise flow in a tee-junction and then became the original 3D post processor for PHOENICS. It is still the author's algorithm of choice and the majority of visualisations presented in this paper have used it.

* Fax: +64 9 373 7479.
E-mail address: g.mallinson@auckland.ac.nz

0017-9310/$ - see front matter © 2009 Elsevier Ltd. All rights reserved.
doi:10.1016/j.ijheatmasstransfer.2009.03.023

Nomenclature

a	arbitrary vector
ds	element of area (m^2)
dv	element of volume (m^3)
e	specific energy (J/kg)
E	total energy transport vector (W/m^2)
f	arbitrary function, or one of the dual stream functions (m^2/s)
f	force per unit mass (N/kg)
g	one of the dual stream functions (m^2/s)
g_{ij}	metric tensor
g	gravitational acceleration vector (m/s^2)
h	heat transfer coefficient (W/m^2K), mesh interval (m)
k	thermal conductivity (W/mK)
p	pressure (N/m^2)
q^i	curvilinear coordinate (m)
q'''	volumetric rate of heat generation (W/m^3)
q	heat flux vector (W/m^2)
$\dot{Q}$	heat flow rate (W)
r	position vector (m)
s	coordinate along a curve (m), specific entropy (J/kgK)
S	entropy transport vector (W/m^2K)
m	mass flux or mass transport vector ($=m_x\mathbf{i} + m_y\mathbf{j} + m_z\mathbf{k}$) ($kg/m^2s$)
M_x	total mass flux through a cell in the *x* direction (kg/s)
Ra	Rayleigh number
t	time (s)
t	tangent vector (m)
T	temperature (K)
v	velocity vector ($=u\mathbf{i} + v\mathbf{j} + w\mathbf{k}$) (m/s)
V	volume (m^3)
λ	arbitrary function
ρ	density (kg/m^3)
ζ	vorticity (/s)
ζ_m	mass vorticity (kg/m^3s)
Ψ_m	2D mass stream function (kg/ms)
$\mathbf{\Psi}$	vector potential for velocity (m^2/s)
$\mathbf{\Psi}_e$	vector potential for the energy transport vector (W/m)
$\mathbf{\Psi}_m$	vector potential for the mass transport vector (kg/ms)
Φ	viscous dissipation function ($/s^2$)
θ	non dimensional Temperature
$\boldsymbol{\sigma}$	deviatoric stress tensor (kg/ms^2)
$\boldsymbol{\tau}$	stress tensor (kg/ms^2)
μ	dynamic viscosity (kg/ms)

Subscripts

b	body (force)
M	mechanical (energy)
m	mass
ref	reference
S	surface
T	temperature or Thermal (energy)
x,y,z	Cartesian coordinates
φ	denotes energy transport vector that includes gravitational potential energy

A major motivation for writing GRAFFIC was the need to have 3D graphics capability for understanding how dual stream functions might be used. GRAFFIC was written for direct view storage tube (DVST) technology which, although interactively inferior to the vector refresh technology that had already been used to construct visualisations of 3D convection, was orders of magnitude less expensive and provided a realistic graphics display technology for industrial CFD/CHT. Eventually GRAFFIC was used much more as a CFD/CHT post processor than it was for dual stream function research.

Ironically, the parabolic and partially parabolic methods developed and used by Brian Spalding's group at that time were, in fact, amenable to dual stream function representation. This was recognised by Brian Spalding who, in the 1990s, tacitly approved of Steven Beale's search for whole field dual stream functions (Beale [6] – chapter 7) described later in this paper.

1.2. Background of issues and problems

What does visualisation mean? In reality is not just graphics or colourful images; there are important conservation laws to represent. When users of CFD solvers and their visualisation methods produce falsely spiralling streamlines, observation clashes with intuition. Unfortunately even today, this is a too common reality. The majority of vector line methods used in commercial software exhibit such artefacts arising from well documented (e.g. Buning [7]) inaccuracies in either path integration or field interpolation.

The original motivation for research into improved algorithms for vector line construction is demonstrated by the natural convection example shown in Fig. 1. The spiral vector line is a streamline for this flow. The smoke visualisation provides clear evidence of the numerically predicted spiralling flow. A 10 cm by 10 cm by 2 cm cavity was heated and cooled by transparent side walls, filled with smoke and then left to settle before illuminating the vertical axial plane. The pattern forms naturally as the slowest moving air loses its smoke particles as they settle on the bottom the cavity thereby forming a continuous sheet of smoke free air. Although there are techniques for modelling smoke dispersion through cavity so that, in principle, the image in Fig. 1(b) could be simulated, a whole field method for constructing stream surfaces and also obviating false spirals is a necessary target if visualisation tools are to have the ability to rapidly define the flow as clearly as the smoke visualisation does.

As reviewed by Mallinson [8] there are several useful visualisation strategies that can be used for very complex 3D and 4D data fields. The present discussion will concentrate on the underlying technology for constructing vector lines. It will also consider the heat line methods proposed by Kimura and Bejan [9] that are of course relevant in the context of computational heat transfer. This paper therefore has two main threads. The first traces the development of research that seeks to find ways to construct the lines of vector fields while accurately maintaining the conservations laws that are represented by their divergence. The second thread considers heat or energy transport lines, their utility and how they may be constructed and used for 3D CFD/CHT fields.

2. Concepts and basic equations

2.1. Preliminaries

To set the mathematical context for the discussions in this paper it is worth reviewing some of the basic concepts associated with the vector fields of fluid dynamics and heat transfer.

An arbitrary vector field, denoted by **a**, may or may not have zero divergence. If it does it is described as being solenoidal. The divergence of **a** is related to the conservation of **a** over a control volume *V* bounded by a closed surface *S* by the Gauss divergence theorem

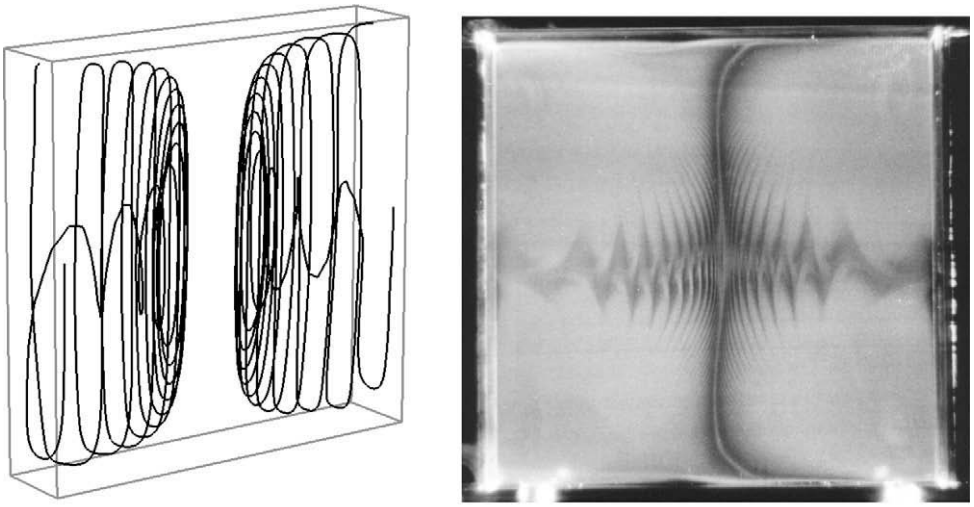

Fig. 1. Natural convection flow in a window cavity. (a) Computed lines of velocity. (b) Smoke visualisation of vector sheets or stream surfaces.

$$\int_V \nabla \cdot \mathbf{a} dV = \oint_S \mathbf{a} \cdot \mathbf{ds}, \tag{1}$$

which says that the total outwards flow of **a** through the bounding surface is equal to the volume integral of the divergence of **a**. Hence if

$$\nabla \cdot \mathbf{a} = f, \tag{2}$$

where f is a scalar function, then

$$\int_V f dV = \oint_S \mathbf{a} \cdot \mathbf{ds}. \tag{3}$$

For a solenoidal vector field $\nabla \cdot \mathbf{a} = 0$ and $f = 0$ so that the net flow of **a** out of the volume is zero. Eq. (1) applies to any volume, and hence applies to each control volume of a finite volume or finite element mesh, any combination of control volumes or the whole solution domain. Eq. (2) is the local representation of the conservation law.

2.2. Mass conservation, mass flux vector, mass vorticity and 2D stream functions

Flow fields are described by the velocity vector, **v**. The conservation of mass can be written as

$$\frac{\partial \rho}{\partial t} + \nabla \cdot \mathbf{m} = 0 : \quad \mathbf{m} = \rho \mathbf{v}. \tag{4}$$

The vector **m** is the mass flux. The form of Eq. (4) identifies **m** as the transport vector for mass a concept that will be generalised in Section 6.

The solenoidal condition for the vector **m** depends on the time rate of change of density. For flows where the Mach number is less than 0.3, **m** can be considered to be solenoidal.

$$\nabla \cdot \mathbf{m} = 0. \tag{5}$$

If the fluid is incompressible the density is constant and the velocity vector, **v**, is solenoidal. Note that whatever the nature of the flow, **m** is locally parallel to **v**.

The vorticity in the flow is defined by

$$\zeta = \nabla \times \mathbf{v}. \tag{6}$$

Because of the usefulness of Eq. (5), it is convenient to define a "mass vorticity" ζ_m by

$$\zeta_m = \nabla \times \mathbf{m}. \tag{7}$$

The vorticity and mass vorticity are related by

$$\zeta_m = \nabla \rho \times \mathbf{v} + \rho \zeta. \tag{8}$$

Initially computational solutions were obtained in 2D, often using the stream function vorticity method. For consistency with later discussions a mass stream function for Cartesian coordinates x and y will be defined here by

$$m_x = \frac{\partial \psi_m}{\partial y} \quad m_y = -\frac{\partial \psi_m}{\partial x}, \tag{9}$$

where m_x and m_y are the x and y components respectively of the mass flux vector. The mass vorticity and stream function are related by

$$\nabla^2_{xy} \psi_m = -\zeta_{m,z} \tag{10}$$

3. Vector potentials and scalar stream functions

A vector field can be derived from vector potentials or scalar stream functions. The term scalar potential is used exclusively here for a function that has its gradient parallel to the vector it is related to. Scalar stream function gradients are normal to the vector they generate.

3.1. Vector potentials

Initial extensions of the vorticity stream function method used a vector potential for velocity. This discussion will use a vector potential for the mass flux vector rather than one for velocity so that

$$\mathbf{m} = \nabla \times \Psi_m \tag{11}$$

As can be readily verified, this representation ensures that **m** is solenoidal.

Taking the curl of (11),

$$\zeta_m = \nabla(\nabla . \Psi_m) - \nabla^2 \Psi_m. \tag{12}$$

If the vector potential is chosen to be solenoidal then

$$\nabla^2 \Psi_m = -\zeta_m, \tag{13}$$

which is analogous to the usual vector potential vorticity equation.

3.2. Dual stream functions

An alternative representation is to use two scalar functions f and g, related to the mass flux vector by

$$\mathbf{m} = \nabla f \times \nabla g. \tag{14}$$

Again, this representation ensures that $\mathbf{m}$ is solenoidal. The functions f and g are called dual stream functions, Yih [10].

Dual stream functions have an important geometrical interpretation. An immediate implication of Eq. (14) is

$$\nabla f \cdot \mathbf{m} = \nabla g \cdot \mathbf{m} = 0. \tag{15}$$

This means that isosurfaces of f and g are stream surfaces for $\mathbf{m}$ (and for $\mathbf{v}$ since $\mathbf{m}$ is parallel to $\mathbf{v}$) as shown in Fig. 3.

Another interpretation of (14) is that it defines a projection from physical space to a 3D coordinate system (f,g,s) where the f and g coordinates are normal to $\mathbf{m}$ and s is in the direction of $\mathbf{m}$, (Fig. 2). Moreover areas in f,g space are proportional to the mass flow rates through areas in physical space. The functions f and g are the true equivalents of the 2D stream function ψ_m. This is contrary to an often expressed impression (e.g. Mahmud and Fraser [11]) that the concept of a stream function is invalid for 3D.

3.3. Relationships between dual stream functions, the vector potential and 2D stream functions

In terms of the 2D mass stream function defined by Eq. (9) the 2D Cartesian stream function ψ_m is equal to the z component of Ψ_m.

Using the conventions here the vector potential can be related to dual stream functions by

$$\Psi_m = f\nabla g \tag{16}$$

By taking the curl of this equation, it can be verified that the vector potential and dual stream function representations of the mass flux vector are equivalent, i.e.,

$$\nabla \times \Psi_m = \nabla \times f\nabla g = \nabla f \times \nabla g + f\nabla \times \nabla g = \nabla f \times \nabla g \tag{17}$$

For 2D flow described in Cartesian coordinates, if $g = z + c$; then for any function f, $f = \psi_m$. The dual stream function representation of 2D in plane flow can also accommodate a through flow, as long as all three components of the mass flux vector depend on only the two in-plane coordinates, (Li and Mallinson [12]). This representation is particularly useful for axisymmetric flows with swirl.

4. Vector lines – streamlines, streak lines and path lines

Visualisation of 3D vector fields is complicated. Vector maps can be constructed on surfaces in a flow and have been popular as the default method for visualising vector fields for several decades. They are far from satisfactory; clarity is difficult to achieve and visualisations soon become very cluttered. The next most obvious method is to construct vector lines that are everywhere tangent to the vector field. Although they can be constructed for any field, the most common are those of the velocity or mass flux fields.

4.1. The construction of vector lines

Given an arbitrary vector, $\mathbf{a}(\mathbf{r},t)$ which is a function of position and time the lines of $\mathbf{a}$ are everywhere tangent to $\mathbf{a}$. Let $\mathbf{r}(s)$ be an arbitrary curve in space where s is a parameter denoting position along the curve. The tangent $\mathbf{t}$ to the curve, is given by

$$\mathbf{t} = \frac{d\mathbf{r}}{ds}, \tag{18}$$

If $\mathbf{t}$ is parallel to $\mathbf{a}$

$$\mathbf{t}(\mathbf{r},t) = \lambda\mathbf{a}(\mathbf{r},t) \Rightarrow \frac{d\mathbf{r}}{ds} = \lambda\mathbf{a}(\mathbf{r},t) \Rightarrow d\mathbf{r} = \lambda\mathbf{a}(\mathbf{r},t)ds, \tag{19}$$

where λ is an arbitrary function.

Now assume that s is a function of t

$$\frac{d\mathbf{r}}{ds} = \frac{d\mathbf{r}}{dt}\frac{dt}{ds} = \frac{1}{\dot{s}}\frac{d\mathbf{r}}{dt} \text{ provided } \dot{s} \neq 0. \tag{20}$$

This leads to

$$\frac{d\mathbf{r}}{dt} = \lambda\dot{s}\mathbf{a}(\mathbf{r},t) \Rightarrow d\mathbf{r} = \lambda\dot{s}\mathbf{a}(\mathbf{r},t)dt. \tag{21}$$

Eq. (21) is the basis for constructing the lines of a vector field. An alternative form of (21) for Cartesian coordinates is

$$\frac{dx}{a_x(\mathbf{r},t)} = \frac{dy}{a_y(\mathbf{r},t)} = \frac{dz}{a_z(\mathbf{r},t)} = \lambda\dot{s}dt. \tag{22}$$

Using either Eqs. (21) or (22) a given line can be constructed by integration from a starting point $(\mathbf{r}_0, t_0)$,

$$\mathbf{r} = \mathbf{r}_0 + \int_{t_0}^{t} \lambda\dot{s}\mathbf{a}(\mathbf{r},\tau)d\tau \tag{23}$$

These equations apply to any field. The first part of this discussion will consider the velocity or mass flux fields. Later, other fields related to the thermal structure of a convection heat transfer process will also be considered.

4.1.1. Stream, path and streak lines

If $\mathbf{a}$ is now replaced by the velocity vector $\mathbf{v}$,

$$\frac{d\mathbf{r}}{dt} \equiv \mathbf{v} \Rightarrow \lambda = \frac{1}{\dot{s}}, \tag{24}$$

and

$$\mathbf{r} = \mathbf{r}_0 + \int_{t_0}^{t} \mathbf{v}(\mathbf{r}(\tau),\tau)d\tau. \tag{25}$$

Streamlines are lines that are constructed tangent to the instantaneous mass flux field at a given time, t_c.

$$\mathbf{r}(s) = \mathbf{r}_0 + \int_{s_0}^{s} \mathbf{m}(\mathbf{r}(\tau),t_c)d\tau. \tag{26}$$

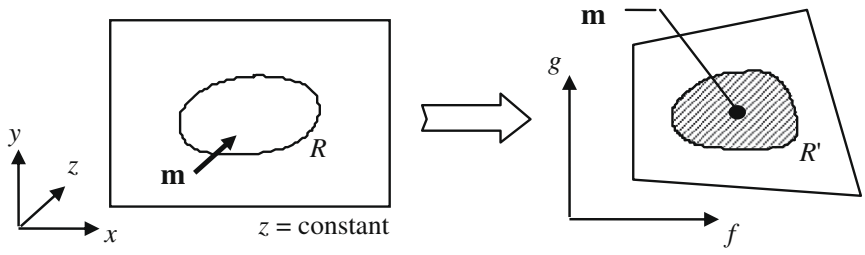

Fig. 2. Dual stream function mapping from physical space to stream function space. The region R on a z = constant plane is mapped into R' in stream function space in which the z axis is directed along the **m** lines.

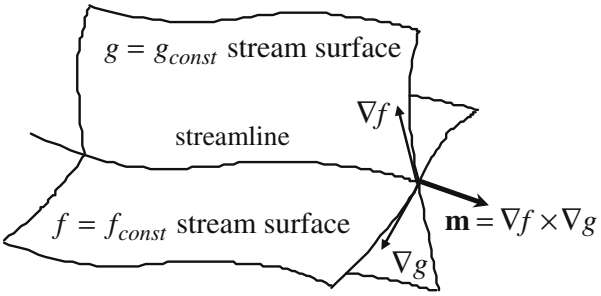

Fig. 3. The relationships between dual stream functions, the vector **m** and its stream surfaces.

Path lines are the paths of elements of fluid. They are defined by applying (25) from a collection of points at a given time. Streak lines are the path lines that all pass through the same point in space, i.e. integrate (25) for the same $\mathbf{r}_0$ for all time. For steady fields the streamlines, path lines and streak lines are identical.

4.1.2. Invariant representation of the solenoidal condition

Before discussing details of various methods for constructing vector lines it is worth considering the behaviour of Eq. (2) with respect to a curvilinear coordinate transformation described by coordinates q^i (the superscript has been used as in standard curvilinear tensor notation). Denote the metric tensor by g_{ij} and $g = \det|g_{ij}|$. Then the divergence of an arbitrary vector **a** can be written as

$$\nabla \cdot \mathbf{a} = \frac{1}{\sqrt{g}} \frac{\partial}{\partial q^i} (\sqrt{g} a^i). \tag{27}$$

Let $\mathbf{b} = \sqrt{g}\mathbf{a}$; then Eq. (27) can be written as

$$\nabla \cdot \mathbf{a} = \frac{1}{\sqrt{g}} \frac{\partial b^i}{\partial q^i} = f. \tag{28}$$

Provided $\sqrt{g} \neq 0$ this can be replaced by

$$\frac{\partial b^i}{\partial q^i} = \sqrt{g} f. \tag{29}$$

For a solenoidal field,

$$\frac{\partial b^i}{\partial q^i} = 0 \Rightarrow \nabla \cdot \mathbf{a} = 0. \tag{30}$$

The physical components of **a** are $a_i^* = \sqrt{g_{ii}} a^i$, hence

$$b^i = \sqrt{\frac{g}{g_{ii}}} a_i^* = \sqrt{g} a^i. \tag{31}$$

This means that in so far as the consideration of the divergence of **a** is concerned, the construction of the vector lines can be discussed in terms of the computational coordinates q^i without losing generality. It will be assumed that computational coordinates are scaled so that they range from 0 to 1 for each cell. It will be understood that the vector field is transformed via Eq. (31).

5. Problems, issues and algorithms that attempt to resolve them

Streamlines for 3D flows first started to appear in the literature in the early 1970s. Holst and Aziz [1] and Mallinson and de Vahl Davis [13] presented streamlines for 3D natural convection and forced flows in enclosures. It was soon realised that the integration method used to numerically evaluate (25) had to be at least 4th order Runge Kutta. The next observation was the velocity component interpolations had to satisfy the solenoidal condition (5) exactly, (Mallinson [14], Mallinson and de Vahl Davis [2]) so as not to introduce false sources that manifest as spiralling lines.

In particular the most common method for interpolating a field within a mesh cell, the trilinear interpolation, does not necessarily satisfy the solenoidal condition. Using the notation of Fig. 4, the trilinear interpolation of the scalar f can be written as,

$$f = \{[f_{000}(1-q^1) + f_{100}q^1]((1-q^2) + [f_{010}(1-q^1) + f_{110}q^1]q^2\} (1-q^3) + \{[f_{001}(1-q^1) + f_{101}q^1]((1-q^2) + [f_{011}(1-q^1) + f_{111}q^1]q^2\}q^3, \tag{32}$$

where q^1, q^2 and q^3 are computational coordinates that have been scaled so that they range from 0 to 1 over the dimensions of a cell. As can be readily verified, using this interpolation for the components of velocity does not, in general, produce a solenoidal vector field within the cell. However, in practice there will be relationships between the mesh values point values of the velocity components that will ensure that at least mass conservation over each cell is satisfied provided the results are properly converged. An interpolation that embodies those relationships may well produce a solenoidal velocity field, but typically those relationships are not available to a visualisation system.

The same comments are also true if an equivalent interpolation is used in an unstructured mesh. Failure to satisfy mass conservation completely is the reason why streamlines traced by many of the major commercial packages may still exhibit false spirals or pass through solid boundaries, although the latter effect may also be attributed to inappropriately large time steps (Buning [7]).

In contrast, mass conservative interpolation is readily achieved when a vector potential is available as part of the solution process. Mallinson [14] used (32) to interpolate the vector potential and then applied $\mathbf{v} = \nabla \times \Psi$ to generate a velocity that automatically satisfied $\nabla \cdot \mathbf{v} = 0$. This had the effect of reducing the complexity of the interpolation by automatically finding combinations of the interpolation coefficients that ensured that the interpolated velocity field was solenoidal.

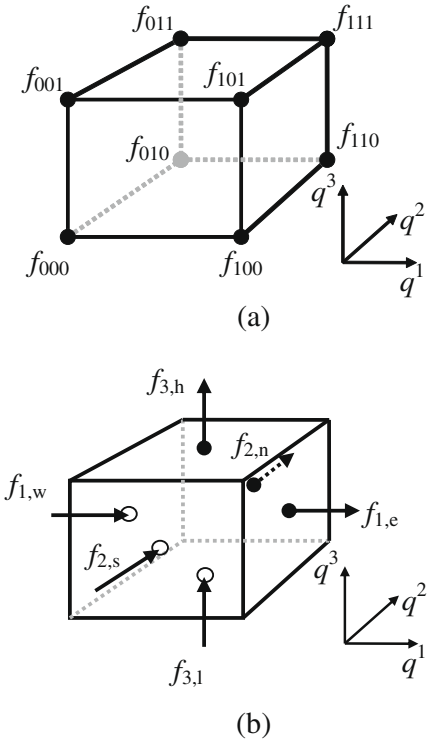

Fig. 4. Notation for data stored at (a) the corners or (b) the face centroids of a hexahedral computational cell.

5.1. Analytical method for advancing through a cell (GRAFFIC algorithm)

An algorithm developed for GRAFFIC (Mallinson [4]) was the first to trace a vector line through a computational cell in a single step. It was written specifically for the face centred staggered grids used by the precursors to PHOENICS. It is assumed by the algorithm that the face centred velocities algebraically satisfy mass conservation. Using the notation in Fig. 4(b), let $M_{x,e}$ denote the total mass flux through the east face of a cell, i.e., $M_{x,e} = f_{1,e}A_e$ etc., following the very familiar PHOENICS style of notation. Assume that this flux varies linearly in the q^1 direction which will be denoted with out loss of generality by x relying on the invariance of the representation of the divergence (30),

$$M_x = M_{x,w} + \frac{(x - x_w)}{(x_e - x_w)}(M_{x,e} - M_{x,w}), \tag{33}$$

with similar expressions for M_y and M_z. The integration of (22) can be separated into individual component equations of the form

$$\frac{dx}{M_{x,w} + \frac{(x-x_w)}{(x_e-x_w)}(M_{x,e} - M_{x,w})} = dt. \tag{34}$$

This has an analytical solution (e.g. for the x direction)

$$x = x_w + \left[\exp\left((t - t_0)\frac{M_{x,e} - M_{x,w}}{x_e - x_w}\right)M_{x,0} - M_{x,w}\right]\frac{x_e - x_w}{M_{x,e} - M_{x,w}}, \tag{35}$$

where the suffix 0 represents either a specified starting point or entry into the cell. The tracking procedure finds the shortest time interval that corresponds to the line traversing the cell and then uses expression (35) to compute the exit coordinates.

This method is still used by the author, although extension to tetrahedra for unstructured grids has not been implemented. It has been used to calculate the bulk of the lines presented in this paper. As discussed in the introduction, the algorithm was implemented in GRAFFIC and it is tightly coupled with the data storage systems used by PHOENICS and other related structured grid codes. The algorithm was described in the open literature by Mallinson [15], but probably has not been incorporated into any commercial code.

5.2. Dual stream functions for whole field visualisation

As discussed in Section 1, dual stream functions have the potential to be used as whole field visualisations since their isosurfaces define stream surfaces in the flow. The issue with their use is demonstrated by the simple analytical example in Fig. 5. The streamline is the intersection of the grey and black isosurfaces. The grey torus is described by a function that is much simpler in its relationship between physical and stream function space than the other function. The function defining the black surface is, in fact, multi-valued in terms of its relationship between points on a streamline and locations in physical space. The grey surface in Fig. 5 defines a closed region of flow and for this reason single valued stream functions were called structural stream functions by Reztsov and Mallinson [16].

For flows where there is no recirculation or spiralling, dual stream functions can be applied for both visualisation and the solutions process. There is a large body of research describing the application of dual stream functions to duct flows (e.g. Greywall [17], Greywall [18], Keller [19]).

5.2.1. Beale's whole field visualisation system

Beale [20] derived equations for relating dual stream functions to the velocity field by taking the cross products of **m** and the gradients of the stream functions. For f,

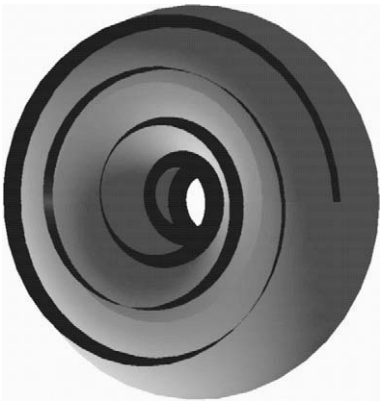

Fig. 5. Simple torus flow example described by analytical dual stream functions. The grey surface is an isosurface of one function the black surface which is an isosurface of the other function describes the spiralling nature of the flow.

$$\mathbf{m} \times \nabla f = (\nabla f \times \nabla g) \times \nabla f = (\nabla f)^2 \nabla g - (\nabla g \cdot \nabla f)\nabla f. \tag{36}$$

Taking the divergence of this equation leads to

$$\nabla \cdot (\mathbf{m} \times \nabla f) = \nabla \cdot ((\nabla f)^2 \nabla g) - \nabla \cdot ((\nabla g.\nabla f)\nabla f). \tag{37}$$

Manipulating the left hand side yields

$$\nabla f \cdot \zeta_m - \nabla \cdot ((\nabla f)^2 \nabla g) + \nabla \cdot ((\nabla g.\nabla f)\nabla f) = 0, \tag{38}$$

and on rearrangement and applying the same steps for g the following pair of equations is produced.

$$\begin{aligned} \nabla \cdot ((\nabla f)^2 \nabla g) &= \nabla \cdot ((\nabla g \cdot \nabla f)\nabla f) + \nabla f \cdot \zeta_m \\ \nabla \cdot \left((\nabla g)^2 \nabla f\right) &= \nabla \cdot ((\nabla g \cdot \nabla f)\nabla g) - \nabla g \cdot \zeta_m \end{aligned} \tag{39}$$

Eqs. (39) are anisotropic diffusion equations that Beale solved using the Spalding whole field solver. The results presented in Beale [20] and Beale [21] show promising definition of the structure of flows around an obstacle and in a free vortex. However, the streamlines for the free vortex do not exhibit spirals that should arise from axial flow and this discrepancy, for which an explanation has not yet been found, remains a topic for future research.

5.3. Dual stream functions for vector line construction

If dual stream functions cannot easily be used for whole field visualisation, then they might be useful for constructing vector lines and surfaces within cells, where the flow can assumed to be simple and non vortical. This approach has been used to successfully trace streamlines for steady flows for structured and unstructured girds.

For a structured grid, each dual stream function is assumed to be interpolated tri-linearly using Eq. (32). Rather than use the interpolations for **m** directly, the approach taken by Kenwright and Mallinson [22] was to construct a representation of the flow through each cell in f,g space and then use that diagram to graphically construct the exit point given an entry or initial point. This process is straightforward because the trilinear interpolation used for f and g preserves straight edges when transforming between computational and stream function spaces. In the diagram in Fig. 6 only two faces enclose the point representing a streamline; one is the inlet face, the other the outlet. This algorithm has been extended for tetrahedral cells in a unstructured mesh by Knight and Mallinson [23] and Li and Mallinson [24] with the latter using higher order interpolations for the stream functions which allow fluid to enter and leave a cell through the same face.

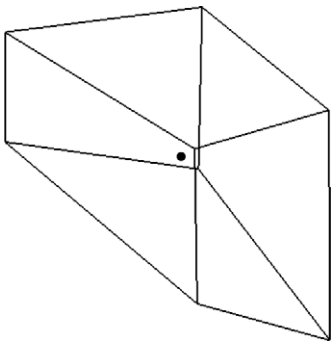

Fig. 6. Dual stream function diagram representing flow through a computational cell. The dot represents a streamline passing through the cell.

Examples of a streamline and vortex lines, in a cubical cavity heated from the side, constructed using the algorithm defined by (35) are presented in Fig. 7(a). The vortex lines correctly close in just one loop through the cavity. Lines constructed using a conventional Runge Kutta integration of a tri-linearly interpolated vorticity field defined at cell corners did not necessarily close after one loop.

Fig. 7(b) has two streamlines; one produced by the analytical algorithm, the other by the dual stream function method. The flow is symmetrical about the central vertical plane so that the stream lines should be mirror images. There are minor differences between the two tracks and this is typical of the performance of different algorithms applied to the same data. Both sets of tracks are, however, perfectly mass conserving. They will not spiral outwards to eventually collide with a boundary. This flow example is also used for the energy transport line visualisations presented later in this paper.

6. Heat or energy transport lines

The previous sections have discussed some of the issues associated with the construction of lines of vector fields. It is now worth considering vector fields other than velocity, mass flux and vorticity that might be of interest in the field of computational heat transfer. For more than two decades there has been a thread of research regarding how heat lines and an associated 2D heat function can be used to visualise heat transfer processes; e.g. Bejan [25], Costa [26,27], Deng and Tang [28,29]. In particular a recent discussion by Mahmud and Fraser [11] has prompted the current investigation of how these methods might be put into a more general visualisation context. The underlying technology is to construct vector fields that are related to a flow/transport process and use those vectors to construct visualisation artefacts.

To date, the heat line methods have concentrated on the lines of fields for which a suitable stream of heat function can be found, thereby limiting the utility of heat lines to 2D flows. The recent work by Mahmud and Fraser [11] has attempted to explore 3D flows by calculating energy path lines. A single 3D path line was presented for steady state natural convection in a cavity heated from the side with $Ra = 10^3$.

6.1. Definition of the energy transport vector

The starting point for this discussion is the conservation of energy equation, the derivation of which can be found in texts such as Bird et al. [30]. Using the Cartesian tensor notation, $\nabla \cdot (\mathbf{v} \cdot \tau) \equiv \frac{\partial}{\partial x_j}(v_i \tau_{ij})$, where τ is the stress tensor ($=-\tau$ in Bird et al. [30]), the equation of energy can be written as

$$\rho \frac{De}{Dt} = q''' - \nabla \cdot \mathbf{q} + \nabla \cdot (\mathbf{v} \cdot \tau) + \rho \mathbf{f}_b \cdot \mathbf{v}, \tag{40}$$

where e is the specific total energy and is equal to the sum of the specific thermal and kinetic (or mechanical) energies.

$$e = e_T + e_M : \quad e_M = \frac{1}{2}|\mathbf{v}|^2. \tag{41}$$

This definition of total energy does not include potential energy and follows the convention used by Bird et al. [30] where the gravitational work is considered to be part of body force work.

Using continuity (4) and separating out the deviatoric stress tensor, $\boldsymbol{\sigma}$,

$$\frac{\partial \rho e}{\partial t} + \nabla \cdot (\rho e \mathbf{v}) + \nabla \cdot \mathbf{q} - \nabla \cdot (\mathbf{v} \cdot \boldsymbol{\sigma}) + \nabla \cdot p\mathbf{v} = q''' + \rho \mathbf{f}_b \cdot \mathbf{v}. \tag{42}$$

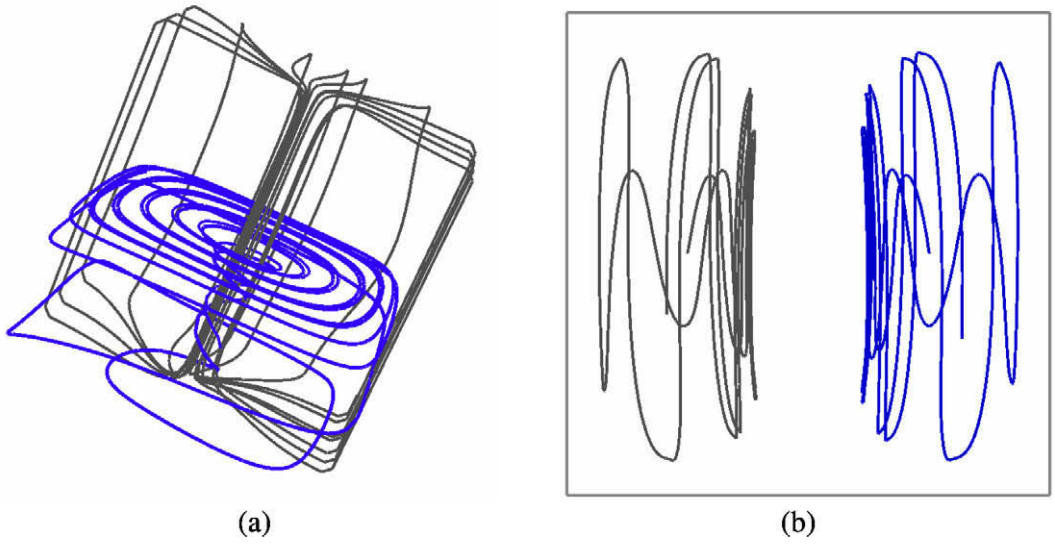

Fig. 7. Visualisations of natural convection in a cubical cavity heated from the side, $Ra = 10^4$ and $Pr = 0.71$. (a) Streamline (blue) and vortex lines (black). The view has been orientated to show the flow. (b) Streamlines constructed using the analytical (black) and dual stream function (blue) algorithms. This flow is corresponds to that represented in Figs. 11 and 12. (For interpretation of color mentioned in this figure the reader is referred to the web version of the article.)

This can be rewritten as

$$\frac{\partial \rho e}{\partial t} + \nabla.\mathbf{E} = q''' + \rho \mathbf{f}_b \cdot \mathbf{v}, \tag{43}$$

where

$$\mathbf{E} = (\rho e + p)\mathbf{v} - (\mathbf{v} \cdot \boldsymbol{\sigma}) + \mathbf{q}. \tag{44}$$

The vector $\mathbf{E}$ is the transport vector for total energy.

If the body force is conservative, say $\mathbf{f} \equiv \mathbf{g} = -\nabla\varphi$, $\mathbf{E}$ can be replaced by

$$\mathbf{E}_\varphi = (\rho e + \rho\varphi + p)\mathbf{v} - (\mathbf{v} \cdot \boldsymbol{\sigma}) + \mathbf{q} = \mathbf{E} + \rho\varphi\mathbf{v}, \tag{45}$$

and (43) becomes

$$\frac{\partial \rho e}{\partial t} + \nabla.\mathbf{E}_\varphi = q'''. \tag{46}$$

If the flow is steady and there is no internal heat generation, the total energy plus potential energy vector is solenoidal,

$$\nabla \cdot \mathbf{E}_\varphi = 0. \tag{47}$$

This vector is the most general energy transport vector that is solenoidal in steady state. It will be referred to here as the *generalised energy transport vector*.

6.2. Energy potentials

The vector potential and scalar function concepts can now be applied to the generalised energy transport vector to create a new energy potentials that encompass the 2D heat function.

6.2.1. Energy dual scalar functions

Let the generalised energy transport vector be represented by two scalar functions

$$\mathbf{E}_\varphi = \nabla f_e \times \nabla g_e. \tag{48}$$

Taking the curl of (48) leads to

$$\begin{aligned}\nabla \times \mathbf{E}_\varphi &= \nabla \times (\nabla f_e \times \nabla g_e) \\ &= (\nabla g_e \cdot \nabla)\nabla f_e - \nabla g_e \nabla^2 f_e - (\nabla f_e \cdot \nabla)\nabla g_e + \nabla f_e \nabla^2 g_e.\end{aligned} \tag{49}$$

For 2D Cartesian situations, let

$$g_e = z\mathbf{k}, \tag{50}$$

then

$$\mathbf{E}_\varphi = \frac{\partial f_e}{\partial y}\mathbf{i} - \frac{\partial f_e}{\partial x}\mathbf{j}, \tag{51}$$

and Eq. (49) becomes

$$\nabla \times \mathbf{E}_\varphi = \frac{\partial^2 f_e}{\partial x \partial z}\mathbf{i} + \frac{\partial^2 f_e}{\partial y \partial z}\mathbf{j} + \frac{\partial^2 f_e}{\partial z^2}\mathbf{k} - \nabla^2 f_e \mathbf{k}. \tag{52}$$

If $\frac{\partial f_e}{\partial z} = 0$ is chosen

$$\nabla \times \mathbf{E}_\varphi = -\nabla^2_{xy} f_e \mathbf{k}: \quad \nabla^2_{xy} = \frac{\partial^2}{\partial x^2} + \frac{\partial^2}{\partial y^2}, \tag{53}$$

which means that f_e corresponds to the heat function used by others and will be called here the energy stream function.

6.2.2. Energy vector potential

An energy vector potential may also be defined,

$$\mathbf{E}_\varphi = \nabla \times \Psi_e: \quad \nabla \cdot \Psi = 0. \tag{54}$$

By taking the curl of (54),

$$\nabla^2 \Psi_e = -\nabla \times \mathbf{E}_\varphi \equiv -\zeta_e, \tag{55}$$

where ζ_e is the "energy vorticity".

It is also possible to represent $\mathbf{E}_\varphi$ by vector and scalar potentials,

$$\mathbf{E}_\varphi = \nabla \times \Psi'_e + \nabla\varphi_e \quad : \quad \nabla^2\varphi_e = \nabla.\mathbf{E}_\varphi \text{ and } \nabla \cdot \Psi'_e = 0 \tag{56}$$

where Ψ'_e may be a different energy vector potential from Ψ_e. This performs the Helmholtz decomposition of a non-solenoidal $\mathbf{E}_\varphi$ into its rotational and irrotational parts and could be used when $\mathbf{E}_\varphi$ is non solenoidal (e.g. unsteady flow, or a non conservative body force).

6.3. Other thermodynamic transport vectors

It is instructive to consider other transport vectors that may be useful. Although Mahmud and Fraser [11] defined an energy flux vector that was similar to the generalised transport vector described above they did not extend the concepts to other transport vectors that may be useful as thermodynamic visualisation aids.

6.3.1. Mechanical energy

The mechanical energy transport vector is defined by

$$\mathbf{E}_M = (\rho e_M + \rho\varphi + p)\mathbf{v} - \mathbf{v}.\boldsymbol{\sigma}. \tag{57}$$

The mechanical energy equation can be taken by forming the inner product of the velocity vector and the momentum equation to produce.

$$\frac{\partial \rho e_{KE}}{\partial t} + \nabla \cdot \mathbf{E}_M = p\nabla \cdot \mathbf{v} - \mu\Phi, \tag{58}$$

or for steady state

$$\nabla \cdot \mathbf{E}_M = p\nabla \cdot \mathbf{v} - \mu\Phi. \tag{59}$$

In general $\mathbf{E}_M$ is not solenoidal; expansion work is a source of mechanical energy and viscous dissipation is a sink.

6.3.2. Thermal energy

The thermal energy transport vector $\mathbf{E}_T$ is defined by

$$\mathbf{E}_T = \rho e_T \mathbf{v} + \mathbf{q}, \tag{60}$$

leading to

$$\mathbf{E}_\varphi = \mathbf{E}_M + \mathbf{E}_T. \tag{61}$$

The thermal energy equation is

$$\frac{\partial \rho e_T}{\partial t} + \nabla \cdot \mathbf{E}_T = q''' + \mu\Phi - p\nabla \cdot \mathbf{v}, \tag{62}$$

and for steady state

$$\nabla \cdot \mathbf{E}_T = \mu\Phi - p\nabla \cdot \mathbf{v}. \tag{63}$$

The thermal and mechanical energy transport vectors are divergence free only when the effects of viscous dissipation and expansion work can be neglected.

6.3.3. Entropy

To derive similar concepts for entropy, the starting point is the entropy equation, (Equation 3.4.11 in Batchelor [31])

$$\rho\frac{Ds}{Dt} = \frac{\kappa(\nabla \cdot \mathbf{v})^2}{T} + \frac{\mu\Phi}{T} - \frac{1}{T}\nabla \cdot \mathbf{q}. \tag{64}$$

Using continuity and rearrangement,

$$\frac{\partial \rho s}{\partial t} + \nabla \cdot \rho s\mathbf{v} + \nabla \cdot \left(\frac{\mathbf{q}}{T}\right) = \frac{\kappa(\nabla \cdot \mathbf{v})^2}{T} + \frac{\mu\Phi}{T} + \nabla\left(\frac{1}{T}\right) \cdot \mathbf{q}. \tag{65}$$

The entropy transport vector $\mathbf{S}$ can be defined as

$$\mathbf{S} = \rho s\mathbf{v} + \frac{\mathbf{q}}{T}. \tag{66}$$

Using $\nabla\left(\frac{1}{T}\right) = -\frac{1}{T^2}\nabla T$

$$\frac{\partial \rho s}{\partial t} + \nabla \cdot \mathbf{S} = \frac{\kappa(\nabla \cdot \mathbf{v})^2}{T} + \frac{\mu \Phi}{T} - \left(\frac{1}{T^2}\right)\nabla T \cdot \mathbf{q}$$
$$= \frac{\kappa(\nabla \cdot \mathbf{v})^2}{T} + \frac{\mu \Phi}{T} + k\left(\frac{\nabla T}{T}\right)^2 \text{ when } \mathbf{q} = -k\nabla T. \quad (67)$$

Note that for steady state conditions **S** is not solenoidal; the right hand side of (67) represents the volumetric rate of entropy production.

7. Thermal energy transport lines for natural convection in a cavity

The example of natural convection in a box heated from the side can be used to discuss the issues involved in using thermodynamic transport vector fields for visualisation and for the ways that these concepts might be used for 3D flows.

The mechanical energy will be considered to be insignificant compared with the thermal energy, and expansion work and viscous dissipation will both be assumed to be negligible leading to the following form of the steady state energy equation.

$$\nabla \cdot e_T \mathbf{v} = -\nabla \cdot \mathbf{q} = \nabla \cdot k\nabla T, \quad (68)$$

and the thermal energy transport vector is given by

$$\mathbf{E}_T = \rho e_T \mathbf{v} + \mathbf{q}. \quad (69)$$

A non-dimensional form of the energy equation is

$$\mathbf{v} \cdot \nabla\theta = \nabla^2\theta, \quad (70)$$

where $\theta = \frac{T - T_0}{(T_1 - T_0)}$ and the density has been assumed to be constant. The non dimensional thermal energy transport vector is

$$\mathbf{E}_T = (\theta - \theta_{\text{ref}})\mathbf{v} - \nabla\theta. \quad (71)$$

The source for the vector potential is

$$\nabla \times \mathbf{E}_T = \nabla \times (\theta - \theta_{\text{ref}})\mathbf{v} = \nabla\theta \times \mathbf{v} + (\theta - \theta_{\text{ref}})\nabla \times \mathbf{v}$$
$$= \nabla\theta \times \mathbf{v} + (\theta - \theta_{\text{ref}})\zeta. \quad (72)$$

7.1. Bejan's example and the issue of the choice of θ_{ref}

The original discussion by Kimura and Bejan [9] presented example heat lines for 2D natural convection in a box heated from the side for $Ra = 1.4 \times 10^5$ and $Pr = 7$. Streamlines and isotherms for these conditions are shown in Fig. 8(a). The other diagrams in Fig. 8 show energy transport lines for three different values of θ_{ref}. In 2D

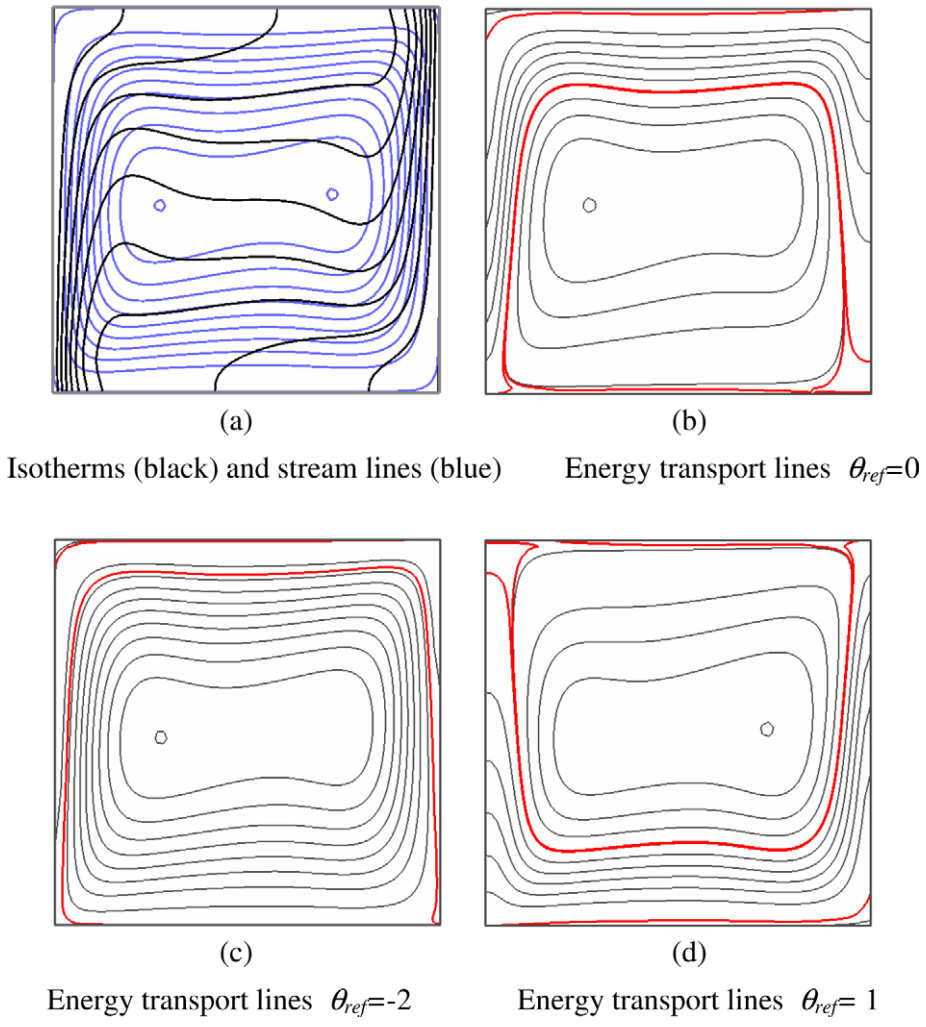

Fig. 8. 2D natural convection in a cavity heated from the left side. $Ra = 1.4 \times 10^5$, $Pr = 7$. Grey contour levels are spaced at 0.1 times the range of energy stream function values. Red contours are for the values −0.06, 0.0 and 5.18 for zero or negative θ_{ref} and 0.0, 5.18 and 5.24 for positive θ_{ref} as explained in the text. (For interpretation of color mentioned in this figure the reader is referred to the web version of the article.)

each line has a value associated with the corresponding energy stream function. The difference between the values of two energy transport lines is equal to the non-dimensional heat flow between them.

The choice of θ_{ref} is arbitrary. It could, for example correspond to the reference conditions for the definition of enthalpy. The convention introduced by Kimura and Bejan [9] has been to use the lowest temperature in a flow domain as the reference temperature, corresponding to $\theta_{ref} = 0$. The energy transport lines in Fig. 8(b) exhibit a recirculation that in fact represents the internal flow of thermal energy stored in the box. If a lower temperature is taken, $\theta_{ref} = -2$ say, then the convection of thermal energy is stronger (Fig. 8(c)). The example, $\theta_{ref} = 1$ has also been included as Fig. 8(d). This reference value has not been used by previous authors, but is equally valid being simply the hottest temperature in the box. In this case the energy recirculation is in the opposite direction.

For this flow, and mesh used, the total non dimensional heat flow through the left wall is 5.24. This was estimated using a second order one sided approximation for the temperature gradient and trapezoidal integration. Because this approximation is different from the central difference approximation used to set the adiabatic condition there is a net heat flow of 0.06 through each "adiabatic boundary". In Fig. 8(b) the 5.18 contour at the top of the box indicates how the hot wall supplies the 0.06 leakage through the top surface. The −0.06 contour leaves the bottom of the right hand wall and circulates around a central core of rotating energy. The 0.06 heat flow that leaves the bottom surface passes around the core to the lowest section of the cold wall. The same observations can be made for Fig. 8(c) but the boundary around the circulating core is much thinner. The energy transport lines in Fig. 8(d) used $\theta_{ref} = 1$ which is the hottest temperature in the cavity. In this case the 5.24 contour separates the heat flow passing through the cavity from the circulating flow.

7.2. Proposed use of the mean temperature as the reference

Another choice for the reference temperature is the mean over the cavity, corresponding to $\theta_{ref} = 0.5$. If this is done the recirculation disappears from the energy transport lines. In Fig. 9(a) the representation of the heat flow is much simpler and, in terms of explaining how the heat flows between the boundaries, the contours have a straightforward interpretation. The heat flow paths between the boundaries can be readily determined. The results for $Ra = 10^6$ and $Pr = 0.71$ confirm that energy transport lines for $\theta_{ref} = 0.5$ show no recirculation at this higher value of Ra. For this flow the non dimensional heat flow through the hot boundary is 9.00 and there is a 0.15 leakage through the horizontal boundaries as delineated by the red contours in Fig. 9(a).

7.3. 3D Energy transport lines

3D solutions for the cavity convection problem were obtained using a vector potential vorticity method and a collocated grid. This method was deliberately chosen so that the velocity and energy transport vector data, defined at cell corners, were not necessarily strictly conservative in the context of cell face fluxes. In order to compare with the results of Kimura and Bejan [9] and Mahmud and Fraser [11] the thermal energy transport vector was calculated using $\theta_{ref} = 0$. Results for $\theta_{ref} = 0.5$ are also presented.

As discussed earlier the analytical vector line method (Eq. (35)) is considered to be the most reliable to prevent false spiralling of vector lines. A technique needed to be found to generate face centred staggered energy transport vector data (Fig. 4(b)) that satisfied global conservation.

7.3.1. Generation of the energy vector potential from collocated energy transport vector data

The method used is described below, and to the author's knowledge this technique has not previously been used in any visualisation context. Although the fluid motion is closed within the cavity, the energy transport vector represents a through flow of energy. At a through flow boundary the condition for Ψ_e is that its curl must represent the flow of $\mathbf{E}_\varphi$ through the boundary. This was achieved by using the auxiliary potential proposed by Hirasaki and Hellums [32]. On a through flow boundary the tangential components of the vector potential were found by solving an equation of the form of (53) with $\mathbf{E}_\varphi$ replaced by Ψ_e and f_e by the auxiliary potential. The source term in this Poisson equation is by Eq. (54) the component of energy transport normal to the boundary.

At the boundaries of the convection cavity, the energy transport vector is equal to the conduction heat flux and its non dimensional value is $\partial\theta/\partial n$ where n is in the direction of the outwards normal. The auxiliary potential is found by solving its Poisson equation and is then used to calculate tangential components of the energy vector potential. At the edges of each boundary the energy vector potential must be continuous and this condition provides enough information to determine a complete set of boundary conditions

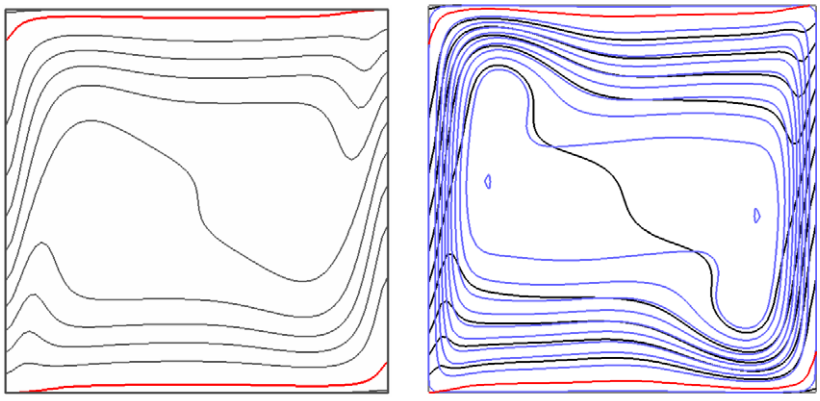

Fig. 9. 2D natural convection in a cavity heated from the left side. Energy transport lines calculated with $\theta_{ref} = 0.5$. (a) $Ra = 1.4 \times 10^5$, $Pr = 7$. Grey contour levels are distributed between −0.061 and 5.24 in 10 equal steps. Red contours are for 0.0 and 5.18. (b) $Ra = 10^6$ and $Pr = 0.71$, Streamlines are blue. Black energy transport lines correspond to contour values uniformly distributed between −0.015 and 9.00. Red contours are 0.0 and 8.85. (For interpretation of color mentioned in this figure the reader is referred to the web version of the article.)

for Ψ_e over all the boundaries of the cavity. Eq. (55) was then solved to produce Ψ_e throughout the cavity.

Given Ψ_e at the mesh nodes in the domain, face centred mass conservative velocity fields can be readily found and these were used as data for the algorithm (35) to produce the lines presented in the following Section.

7.3.2. Example energy transport lines

Heat lines for $Ra = 10^3$, $Pr = 0.71$ and $\theta_{ref} = 0$ are presented in Fig. 10. This is virtually the same as the example presented by Mahmud and Fraser [11]. The lines in Fig. 10, however, appear to describe a vector field that is different from that suggested by the single line in Fig. 11 of Mahmud and Fraser [11]. That path line was launched near the low z, low y corner of the hot wall, spiralled on the $y = 0$ wall, then along the cavity centreline and finally outwards near the $y = 0.5$ plane to eventually leave the cavity via the cold wall. Because the fluid adjacent to the $y = 0$ wall is stationary, the heat lines there should be nearly horizontal. For $Ra = 10^3$ convection is weak and the influence of the wall is felt for some distance from it. The rake of lines in Fig. 10(a) confirms this expectation and the lines spiral only far from the wall. The fact that the line constructed by Mahmud and Fraser [11] is spiralling very close to the $y = 0$ wall is inconsistent with the boundary conditions.

For this value of Ra there is no completely closed recirculation of energy within the cavity. There is a small region of spiralling energy transport lines that are fed from the edge between the heated wall and the end adiabatic wall. This spiralling energy flow proceeds to the central symmetry plane where it spirals outwards to exit the cavity via the cold wall.

If the Rayleigh number is increased the spiralling flow becomes stronger as illustrated in Fig. 11 for $Ra = 10^4$. In this case there is a single small annular region of recirculation identified by the grey energy transport lines.

As was the case for the 2D flows, using $\theta_{ref} = 0.5$ removed the recirculation. The rakes presented in Fig. 12 indicate that the influence of the end walls propagates strongly through the cavity. The $z = 0.25$ rake indicates that the flow has the most influence on the heat lines in the region of $y = 0.25$ which corresponds to the

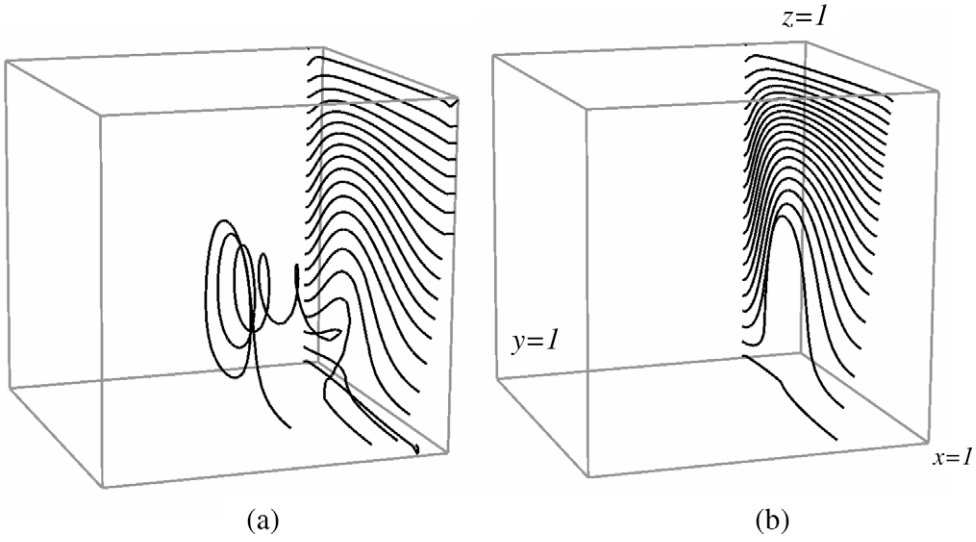

Fig. 10. Energy transport lines for 3D convection in a box with $Ra = 10^3$ and $Pr = 0.71$. The rear wall is heated and the front one cooled. (a) A rake of lines launched from $y = 0.05$ on the heated surface. (b) A rake of lines launched from $y = 0.2$. The flow is symmetrical about $y = 0.5$.

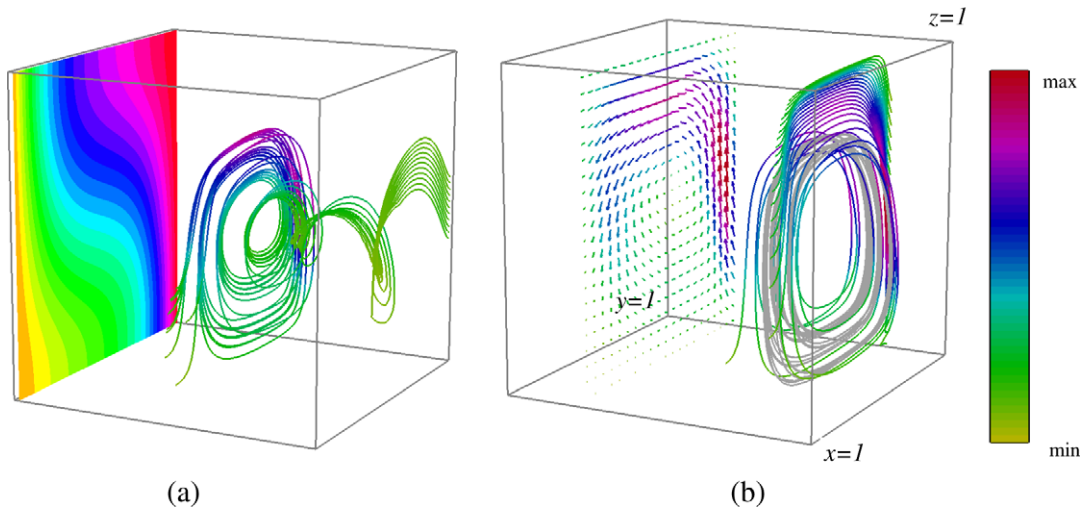

Fig. 11. Energy transport lines for $Ra = 10^4$ and $Pr = 0.71$. The back wall is heated. (a) Rake of lines leaving from $y = 0.01$ on the heated wall. (b) Rake leaving from $y = 0.2$ on the heated wall. Vector map on $y = 0.8$; the grey energy transport lines identify the self contained region of energy transport recirculation. (For interpretation of the references to colour in this figure legend, the reader is referred to the web version of this article.)

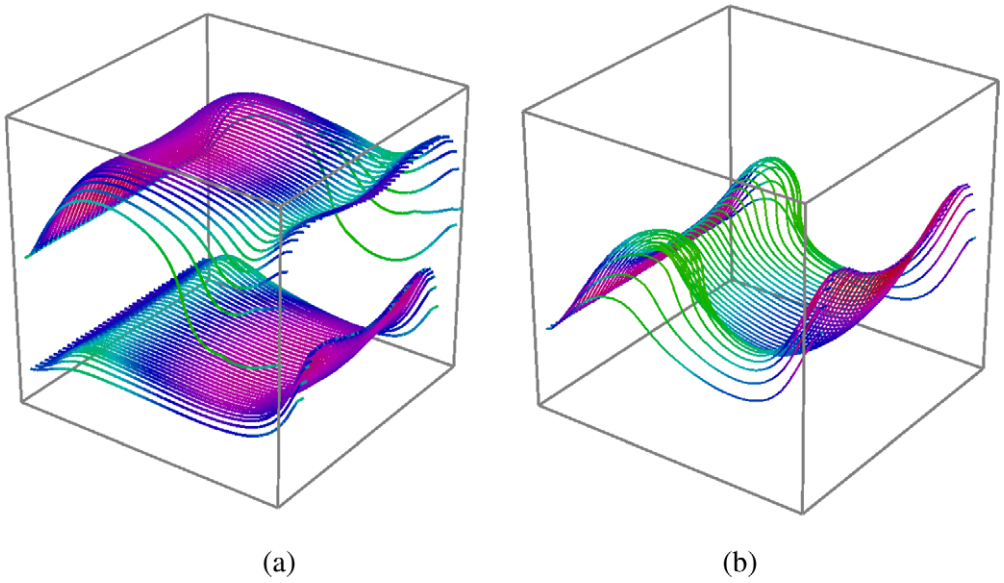

Fig. 12. Energy transport lines for $Ra = 10^4$ and $Pr = 0.71$, and $\theta_{ref} = 0.5$. (a) Rakes leaving from 0.1 and 0.5 up the heated wall. (b) Rake leaving from 0.25 up the heated wall.

strong recirculation region identified in Fig. 11 for the $\theta_{ref} = 0.0$ heat lines (fluid motion for this flow is shown in Fig. 7).

8. Conclusion

The first sections of this paper reviewed methods that use a vector potential or scalar stream functions to ensure that numerically constructed vector lines properly represent the vector field's divergence particularly when it is zero. Consideration of vector fields that may facilitate the understanding of heat and mass transfer processes has led to the suggestion of a generalised energy transport vector which for steady flows in a conservative body force field is solenoidal. This vector is the sum of mechanical energy and thermal energy transport vectors that may not, in general, be individually solenoidal. An entropy transport vector has also been suggested. The lines of these transport vectors are generalisations of the heat lines proposed by Kimura and Bejan [9].

While thermodynamic transport vectors may potentially be useful for visualisation, it is necessary to re-consider the conventions used to define the reference for temperature in the energy transport vector's convection term. The fact that the choice of θ_{ref} has a significant influence on the form of the energy transport vector field is of some concern from a visualisation point of view and may limit the widespread acceptance of the energy transport vector as an interpretive quantity. If any value other than the mean temperature is chosen, then the 2D solutions exhibit energy recirculation. For the 3D flows, the energy vector lines indicate that the circulating region is much smaller than for the corresponding 2D case.

Regardless of the chosen reference temperature there is still the issue of providing divergence preserving data for vector line construction. Whereas fields produced by a computational heat transfer solver may satisfy conservation those produced by a post processing algorithm may not. For the examples presented here, an energy vector potential was derived from the energy transport vector and used to generate cell face centred data. The resulting set of visualisations, which are the most comprehensive heat or thermal line visualisations for a 3D problem presented to date, provide thought provoking visualisations.

This discussion has traced visualisation developments that stem from the author's association with Brian Spalding in the mid 1970s. The desire to provide rigorous visualisations of the face centred velocity fields led to the development of a mass conservative streamline tracing procedure and to the GRAFFIC visualisation software. This thread of development has continued with the search for methods that may produce complete visualisations of the structure of a 3D flow and the work of Beale [20] which was also influenced by Brian Spalding has been a step in this direction. It is perhaps fitting that at the time of Brian Spalding's 85th birthday vector and scalar potentials may emerge has having relevance to ensure that visualisations of generalised transport vectors accurately satisfy the conservation laws they represent.

References

[1] P.H. Holst, K. Aziz, Transient three dimensional natural convection in confined porous media, Int. J. Heat Mass Transfer 15 (1) (1972) 73–90.
[2] G.D. Mallinson, G. de Vahl Davis, Three dimensional natural convection in a box: a numerical study, J. Fluid Mech. 83 (1) (1977) 1–31.
[3] D.B. Spalding, A general purpose computer program for multi-dimensional one- and two phase flow, Math. Comput. Simul. 23 (3) (1981) 267–276.
[4] G.D. Mallinson, GRAFFIC – The Graphical Representation and Analysis of Fluid Flow by Interactive Computation: Software Documentation, Concentration Heat and Momentum Ltd, 1977.
[5] A. Pollard, D.B. Spalding, The prediction of the three-dimensional turbulent flow field in a flow-splitting tee-junction, Comput. Methods Appl. Mech. Eng. 13 (3) (1978) 293–306.
[6] S.B. Beale, Fluid Flow and Heat Transfer in Tube Banks, PhD thesis, University of London, 1993.
[7] P.G. Buning, Sources of error in the graphical analysis of CFD results, J. Sci. Comput. 3 (2) (1987) 149–164.
[8] G.D. Mallinson, CFD visualisation: challenges of complex 3D and 4D data fields, Int. J. Comput. Fluid Dyn. 22 (1) (2008) 49–59.
[9] S. Kimura, A. Bejan, The "Heatline" visualization of convective heat transfer, ASME J. Heat Transfer 105 (1983) 916–919.
[10] C.S. Yih, Stream functions in three-dimensional flows, La Houlle Blanche 3 (1957) 445.
[11] S. Mahmud, R.A. Fraser, Visualizing energy flows through energy streamlines and pathlines, Int. J. Heat Mass Transfer 50 (2007) 3990–4002.
[12] Z. Li, G. Mallinson, Visualising streamlines for 3D fluid momentum with two variables using dual stream functions, Comput. Vis. Sci. 9 (1) (2006) 33–41.
[13] G.D. Mallinson, G. de Vahl Davis, The method of the false transient for the solution of coupled elliptic equations, J. Comput. Phys. 12 (4) (1973) 435–461.
[14] G. Mallinson, Natural Convection in a Box, PhD thesis, University of New South Wales, Sydney, 1973.
[15] G.D. Mallinson, The calculation of the lines of a three-dimensional vector field, in: G. de Vahl Davis, C. Fletcher (Eds.), Computational Fluid Mechanics, North Holland, 1986, pp. 525–534.
[16] A.V. Reztsov, G.D. Mallinson, Dual stream functions for 3D swirling flows, in: 13th Australasian Fluid Mechanics Conference, Sydney, 1998, pp. 179–182.
[17] M.S. Greywall, Streamwise computation of three-dimensional incompressible potential flows, J. Comput. Phys. 78 (1988) 178–193.

[18] M.S. Greywall, Streamwise computation of three-dimensional flows using two stream functions, J. Fluids Eng. 115 (1993) 233–238.
[19] J.J. Keller, A pair of stream functions for three-dimensional vortex flows, Z. Agnew. Math. Phys. 47 (1996) 821–836.
[20] S.B. Beale, A numerical scheme for the generation of streamlines in three dimensions, in: CFD93, Conference of the CFD Society of Canada, Montreal, 1993, pp. 289–300.
[21] S.B. Beale, Visualisation of three-dimensional flow fields using two stream functions, in: 10th International Symposium on Transport Phenomena, Kyoto, Japan, 1997.
[22] D. Kenwright, G. Mallinson, A 3-D streamline tracking algorithm using dual stream functions, in: IEEE Visualization '93, Boston, 1993.
[23] D. Knight, G. Mallinson, Visualising unstructured flow data using dual stream functions, IEEE Trans. Vis. Comput. Graph. 2 (4) (1996) 355–363.
[24] Z. Li, G.D. Mallinson, Dual stream functions for linearly varying momentum vector fields over tetrahedral domains, in: 10th International Symposium on Flow Visualization, Kyoto, Japan, 2002, paper F0121.
[25] A. Bejan, Convection Heat Transfer, third ed., John Wiley & Sons, Inc., 2004.
[26] V.A.F. Costa, Unified streamline, heatline and massline methods for the visualization of two-dimensional heat and mass transfer in anisotropic media, Int. J. Heat Mass Transfer 46 (2003) 1309–1320.
[27] V.A.F. Costa, Bejan's heatlines and masslines for convection visualization and analysis, Trans. ASME Appl. Mech. Rev. 59 (2006) 126–145.
[28] Q.H. Deng, G.F. Tang, Numerical visualization of mass and heat transport for mixed convective heat transfer by streamline and heatline, Int. J. Heat Mass Transfer 45 (2002) 2387–2396.
[29] Q.H. Deng, G.F. Tang, Numerical visualization of mass and heat transport for conjugate natural convection/heat conduction by streamline and heatline, Int. J. Heat Mass Transfer 45 (2002) 2373–2385.
[30] B.R. Bird, W.E. Stewart, E.N. Lightfoot, Transport Phenomena, second ed., John Wiley & Sons, Inc., 2006.
[31] G.K. Batchelor, An Introduction to Fluid Dynamics, Cambridge University Press, 1967.
[32] G.J. Hirasaki, J.D. Hellums, A general formulation of the boundary conditions on the vector potential in three-dimensional hydrodynamics, Q. Appl. Math. 26 (1968) 331–342.